Soft Matter

PAPER

Effects of attraction strength on microchannel flow of colloid–polymer depletion mixtures†

Rahul Pandey[a] and Jacinta C. Conrad*[ab]

We investigated the effect of the strength of the interparticle attraction on the flow properties and microstructure of colloid–polymer depletion mixtures during microchannel flow. When the strength of the interparticle attraction is increased, the additional elasticity imparted by the formation of interparticle bonds does not modify the magnitude of the flow velocities downstream, but instead leads to changes in the flow profiles near the edges of the microchannel that reflect yielding at the weak bonds between clusters. As a result, increasing the strength of attraction increases the resistance of the suspension to densification and to shear-induced migration.

Introduction

Adding an interparticle attraction to colloidal particles modifies the bulk rheological properties of the resulting suspension. When particles interact only *via* a hard-sphere or repulsive interaction, the viscosity of the suspension increases with increasing shear rate ("shear thickening").[1–3] As the strength of the interparticle attraction is increased, the formation of bonds between particles reduces the extent of shear thickening.[4] When the strength of the interparticle attraction[5–7] or the volume fraction[8] become sufficiently large, the suspension undergoes a fluid-to-solid transition that is driven by the formation of an interconnected network of particles.[9] In non-dilute suspensions (typically when the volume fraction of particles $\phi > 0.1$) the network is composed of dense nonfractal clusters of particles[10] whose structure and size depend upon the strength and range of the attraction.[11] Breaking the relatively weak bonds between clusters leads to yielding of the network[12] and hence to flow,[60,61] and thus the clusters control the macroscopic mechanical properties of the suspension.[13,14]

In contrast to the bulk rheology of suspensions, which has been extensively reviewed,[15–18] the rheological properties of suspensions confined in one or more dimensions have received comparatively little attention. Nonetheless, understanding how confinement modifies flow properties is paramount for applications that exploit flows of attractive micro- and nanoparticle suspensions in confined geometries. For example, inkjet printing[19,20] and direct ink-writing[21] of metallic nanocolloidal suspensions enable rapid deposition of conductive microscale wires; semisolid flow batteries[22] use conductive colloidal

suspensions as flowable electrodes; and the thermal conductivity of nanofluids used as coolants increases with agglomeration.[23,24] As these suspensions are flowed through increasingly fine geometries, the presence of nearby walls and surfaces induces frictional interactions and wall slip[25,26] that lead to non-uniform flows and clogging.[27] Reducing the feature sizes for these applications while maintaining the particle connectivity required for conductivity requires tuning the interparticle interactions to minimize clogging and jamming. In turn, this goal requires investigations that correlate microstructure to flow properties of attractive suspensions in confined geometries. However, materials traditionally used as confining geometries, such as packings of spherical beads,[28,29] exhibit locally disordered structures that complicate both measurement and interpretation of the flow properties on the microscale. In addition, such materials are often opaque, which precludes direct imaging and visualization of the microstructure of the suspension.

Microfluidics[30] offers a convenient platform that circumvents the limitations on studies of confined flow imposed by traditional materials. Enabled by advances in microfabrication, well-controlled geometries can be assembled from glass capillaries[31] or fabricated from elastomers using soft lithography.[32] In these transparent geometries, the structure of particles can be directly visualized using optical[33] or confocal[34] microscopy. Indeed, microfluidic techniques have been extensively applied to study the flow properties of concentrated suspensions in which the particles interact *via* hard-sphere or repulsive interactions. For example, microchannel flows have enabled investigations of shear-induced migration in both monodisperse[35] and bidisperse[36] suspensions, and of intermittent flows in glassy suspensions in which the formation of bridges between particles[37,38] leads to self-constriction.[39] The latter flows are reminiscent of those observed in constricted geometries,[40] in which walls can induce changes in the local ordering of particles. Finally, the local velocity profiles have been quantitatively correlated to the rheological properties of the suspension.[41]

[a]*Department of Chemical & Biomolecular Engineering, University of Houston, Houston, Texas, USA. E-mail: jcconrad@uh.edu*
[b]*Petroleum Engineering Program, University of Houston, Houston, Texas, USA*

In attractive suspensions, interactions between particles and between particles and walls must modify the confined flow properties. For example, colloidal suspensions with a strong and short-ranged hydrophobic attraction flowing in microchannels exhibited plug-like velocity profiles, in which the velocity at the center of the channel was nearly constant.[42] Similarly, the velocity profiles of polyelectrolyte-bridged colloidal gels in microchannels exhibited a transition from plug-like to fluid-like[43,44] as the flow rate was increased. The shear rate at the plug-to-fluid transition coincided with that for yielding of the bonds between particles, as determined by bulk rheological measurements.[43] However, the attractive suspensions in these studies have limited applicability as models because of the poor control over the effective attractions afforded by these mechanisms of gelation. General insight into the relationship between microstructure and confined flow properties in attractive colloidal suspensions thus requires investigations in which the strength of the interparticle attraction can be carefully controlled.

Here, we use microfluidics to investigate the effects of attraction on the structure of colloidal particles during confined flow. Using confocal microscopy, we image the flow of colloid–polymer depletion mixtures, which serve as models for a variety of attractive suspensions, during microchannel flow. By changing the concentration of the depletant polymer, we controllably tune the strength of the interparticle attraction. The bulk viscosity of suspensions with either a weak or a strong interparticle attraction decreases with increasing shear rate, typical of weak viscoelastic fluids. However, we find that the strength of attraction modifies the extent of consolidation during microchannel flow. We measure both velocity and density profiles at multiple positions along the microchannel and show that the elasticity imparted by strong attractions suppresses both densification and shear-induced migration. Our results provide new insight into how interparticle attractions modify the structure of suspensions during confined flow in two technologically relevant limits of the strength of attraction.

Experimental methods

Sample preparation

To create suspensions with controlled interparticle attractions, we synthesized nearly hard-sphere[45] poly(methylmethacrylate) (PMMA) colloidal particles that are stabilized by short poly-(12-hydroxysteric acid) (PHSA) polymers.[46] During synthesis the particles were fluorescently labeled with Nile red, which is excited by light of wavelength $\lambda = 561$ nm. After synthesis, we repeatedly washed the particles in decahydronaphthalene (DHN) to remove any excess dye that is not incorporated into the particles. The diameter of our particles was $2a = 1.546$ μm and the polydispersity was 0.0488, as measured using dynamic light scattering (Brookhaven Instruments, BI-APD). The particles were suspended in a solvent mixture of cyclohexyl bromide (CXB) and DHN (75.7% and 24.3% by weight, respectively) that very nearly matches both their density ($\rho \approx 1.22$ g mL^{-1}) and their index of refraction ($n \approx 1.49$). We further minimized the effects of gravity by adding CXB or DHN dropwise (10 μL) to all samples (6 mL) and confirmed that the particles remained in suspension after centrifugation at $800g$ and 25 °C for 1.25 h; this protocol ensured

that the buoyancy mismatch between the particles and the solvent was $\Delta\rho < 1.4 \times 10^{-3}$ mg mL^{-1} at the temperature at which experiments were performed, 24.7 ± 0.7 °C. To mitigate the slight electrostatic repulsion between the particles in these solvents, we added 1.5 mM of an organic salt, tetrabutyl-(ammonium chloride) (TBAC),[47] which partially screened the charges on the particles. To induce an attraction of controlled range and strength between the particles, we added non-adsorbing linear polystyrene (PS) of molecular weight $M_w = 295\,800$ kDa (Bangs Labs). The radius of gyration of the polymer in the solvent mixture was $R_g \approx 15$ nm (ref. 48) and the overlap concentration was $c_p^* = 3M_w/4\pi R_g^3 N_A \approx 35$ mg mL^{-1}. The polymer concentration sets the strength of attraction $U(r) = -\Pi_p V_o$ (for $2a < r < 2a + 2R_g$), where V_o is the overlapping volume of the depletion zone between two particles and the osmotic pressure $\Pi_p \propto n_p^{(R)}$ is linearly proportional to the number density of polymers in the free volume.[49] Here we held constant the volume fraction of the colloidal particles ($\phi \approx 0.15$) and varied the strength of attraction by changing the concentration of polymer c_p. We investigated two suspensions: one in which the particles interact via a weak attraction ($\phi = 0.155$ and $c_p = 5$ mg mL^{-1}, $U \sim \mathcal{O}(1\,\text{kT})$) and one with a strong interparticle attraction ($\phi = 0.150$ and $c_p = 25$ mg mL^{-1}, $U \sim \mathcal{O}(10\,\text{kT})$). These two limits model the strengths of the interparticle attraction in flowable electrolytes[22] and in ink feedstocks,[21] respectively, allowing us to investigate the relationship between microstructure and confined flow properties in a range of technologically relevant conditions.

Bulk rheology

To determine the relationship between viscosity and shear rate, we measured the nonlinear flow curves for our suspensions using a controlled-stress rheometer (Anton-Paar, MCR302) equipped with a double-wall Couette geometry (DG26.7) to maximize the accessible range of torques. The bob length of this geometry is 40 mm and the gap width is 0.42 mm. Prior to measurements, samples were sheared at a steady shear rate of 300 s^{-1} for 60 s to remove any shear history and allowed to age for 5 min. We measured the apparent viscosity of the suspension η and the shear stress σ as a function of the shear rate over the range of 10^{-3} to 10^3 s^{-1}, which includes the shear rates experienced by the suspensions during microchannel flow.

Microchannel flow experiment

We acquired images of the colloidal suspensions during flow using confocal microscopy. Our setup consists of a VT-Eye line-scanning confocal scanhead (Visitech, Sunderland, U.K.) that is mounted on an inverted Leica DMR-4000 microscope equipped with a 100× oil-immersion objective (NA = 1.40). We fabricated a simple microfluidic device in which to investigate the confined flow properties of our suspensions, as shown in the schematic in Fig. 1. A glass microcapillary of square inner cross-section (side length $L = 100$ μm) and length 5 cm (Vitrocom, MountainLakes, NJ) was attached to Teflon tubing of length 160 mm (26 AWG, 0.016 in ID × 0.003 in wall, Zeus PTFE Sublite wall tubing, SmallParts.com) on both ends. One end of the tubing was connected to a syringe pump (Micromate, Cadence Science, Staunton, VA) that operates

at constant displacement. For these experiments, we varied the volumetric flow rate between 8 and 30 μL h^{-1}, which yielded velocities of the order of magnitude of 100 μm s^{-1} in the microchannel; we were unable to achieve steady flow at lower volumetric flow rates, as the suspensions repeatedly clogged and jammed the microchannel. The high velocities of the particles precluded full three-dimensional imaging of individual colloids during flow. Instead, we acquired sequential two-dimensional movies of 500 images at a frame rate of 32 frames per second at ten different heights in the sample ($z = 5$ to 50 μm above the bottom surface of the microchannel, corresponding to $z/L = 0.05$–0.5 channel diameters) in the sample. This protocol allowed us to simultaneously measure the velocity profiles, using image correlation algorithms, and locate the particle positions, using particle-tracking algorithms. We acquired movies at different positions $x = 5$ mm to $x = 20$ mm downstream along the microchannel, corresponding to $x/L = 50$–200 channel diameters downstream.

Image analysis

To obtain information about the spatial arrangement of particles during flow, we used standard algorithms[50] implemented in Matlab[51] (MathWorks, Natick, MA) to locate the centroids of the particles in two dimensions. The resolution of the centroid finding algorithm for our particles was 40 nm, as determined from the y-intercept of a plot of the mean-square displacement as a function of time measured for a quiescent sample. To determine the number density of particles, we first located the particles in each image of each movie and then calculated the average number of particles in horizontal slices of constant height (constant y as indicated in the schematic in Fig. 1). We report the mean and standard deviation of the resulting histogram as the number of particles. We converted the number of particles into a volume fraction following the protocol of Semwogerere *et al.*[35] We measured the number density at ten fixed heights separated by a constant spacing $\Delta z = 5$ μm, which is greater than the diameter of the particles. We therefore estimated the bulk volume fraction as

$$\phi_{bulk} = \frac{\left(N \bigg/ \frac{2a}{\Delta z}\right) \frac{4}{3}\pi a^3}{L_x L_y L_z} \tag{1}$$

where L_x and L_y are the length and width of each image slice and $L_z = n_{slices}\Delta z$ is the total height of the image stack. This method of estimating ϕ_{bulk} was previously reported to agree with the bulk volume fraction within an error of 5% when compared to that obtained by full 3-D tracking.[35]

The colloidal particles in our experiments typically moved distances that were greater than the interparticle separation between consecutive frames, and thus standard algorithms for tracking the positions of the particles could not be used to obtain the advection velocities. Instead, the advection velocity across the microchannel was calculated using image correlation algorithms (reviewed in ref. 52) that we implemented in Matlab. Briefly, we subdivided our image into horizontal slices of constant height (y) along the direction of flow (x). For two sequential images $I_1(x,y)$ and $I_2(x,y)$ we first shifted the latter image by a factor Δx and then calculated the cross-covariance between $I_1(x,y)$ and $I_2(x + \Delta x,y)$. For each horizontal slice we determined the shift factor Δx that maximized the cross-covariance between the pair of images, and confirmed that the flow was steady by measuring the slope of the shift factors over time. We then calculated the histogram of Δx obtained for all pairs of consecutive images in a microscopy movie. This histogram typically exhibited a strongly peaked maximum at a particular value of the shift factor Δx. We therefore report the mean and standard deviation of this distribution as the advection velocity and associated error at each lateral position y.

Results and discussion

We characterize the bulk mechanical properties of suspensions at a constant volume fraction $\phi = 0.15$ by measuring the apparent viscosity η and shear stress σ as a function of the shear rate $\dot{\gamma}$. Suspensions with a low concentration of polymer ($c_p = 5$ mg mL^{-1}) exhibit shear-thinning rheology, as shown by the circles in Fig. 2. The viscosity decreases with increasing shear rate until it reaches a final plateau at a shear rate $\dot{\gamma} \approx 1$; as $\dot{\gamma}$ is further increased, the viscosity remains nearly constant over three orders of magnitude in shear rate. When the concentration of the polymer is increased to $c_p = 25$ mg mL^{-1} the viscosity of the suspension increases at all
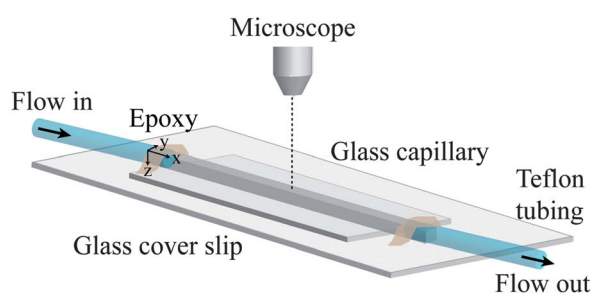

Fig. 1 Schematic of device for microchannel flow experiments, which consists of a glass microcapillary that is attached to a syringe pump using Teflon tubing. The schematic as shown is inverted compared to the experimental setup, which uses an inverted microscope. The coordinate system is indicated: x is oriented along the direction of flow, y is oriented along the width of the microchannel, and z is oriented along the vertical direction.
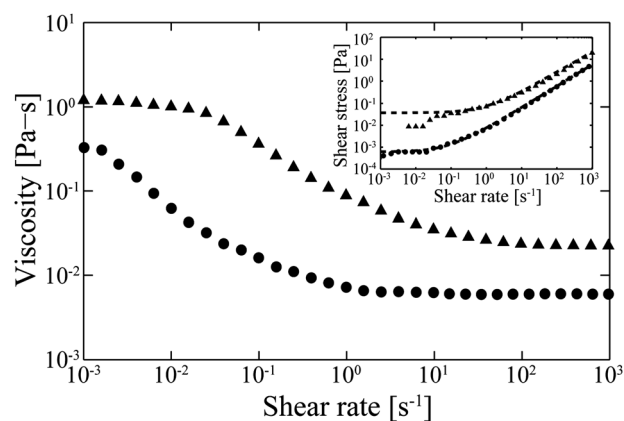

Fig. 2 Viscosity as a function of shear rate for attractive colloidal suspensions with $c_p = 5$ (circles, weak attraction) and 25 (triangles, strong attraction) mg mL^{-1}. Inset: shear stress *versus* shear rate; the dashed lines indicate fits to the Herschel–Bulkley model.[53]

shear rates, as shown by the triangles in Fig. 2, and the shear rate at which the final Newtonian plateau is reached increases to $\dot{\gamma} \approx 10$. At low shear rates, the stress appears to reach a plateau and then decreases further at the lowest shear rates, indicating that the suspension undergoes slip.[26] We fit the rheological data for both samples using the Herschel–Bulkley model,[53] in which the shear stress as a function of the shear rate is given by $\sigma = \sigma_y + k\dot{\gamma}^n$; here σ_y is the yield stress, k is the consistency index, and n is the shear-thinning exponent. For the strongly attractive suspension ($c_p = 25$ mg mL^{-1}) we obtain $\sigma_y = 3.7 \times 10^{-2}$ Pa, $k = 0.039$ Pa s, and $n = 0.91$; for the weakly attractive suspension ($c_p = 5$ mg mL^{-1}), we obtain $\sigma_y = 6.1 \times 10^{-4}$ Pa, $k = 7.0 \times 10^{-3}$ Pa s, and $n \approx 0.97$. We note that for the maximum estimated gravitational mismatch between the solvent mixture and the particles ($\Delta\rho < 1.4 \times 10^{-3}$ mg mL^{-1}), the gravitational stress over the diameter of the micro-capillary used in the flow experiments ($\Delta z \approx 100$ μm), estimated from Darcy's law at short times,[54] is $\sigma \approx \Delta\rho g \phi \Delta z \approx 2 \times 10^{-4}$ Pa. The magnitude of the gravitational stress is comparable to the yield stress for the weakly attractive suspension, suggesting that structures in this suspension cannot withstand even the weak gravitational stresses. The bulk rheology measurements thus indicate that the particles in the strongly attractive suspension form an interconnected network that yields at high stresses, whereas the particles in the weakly attractive suspension are dispersed.

We confirm these structural predictions from the bulk rheological measurements by directly imaging the colloidal suspensions in quiescent conditions and during flow in microchannels using confocal microscopy. Representative micrographs show that increasing the strength of attraction dramatically modifies the microstructure of the suspension, as shown in Fig. 3. For the weakly attractive suspension (Fig. 3(b–d)) flowing at a volumetric flow rate of 8 μL h^{-1}, the particles are distributed nearly

isotropically throughout the channel. By contrast, the strongly attractive suspension (Fig. 3(f–h)) contains distinct clusters that are formed when the flow-induced stresses disrupt the gel network (Fig. 3(e)). We predict that these distinct microstructures will affect both the flow profiles and the distribution of particles during microchannel flow.

As a simple demonstration of this prediction, we show that the strength of the interparticle attraction affects the bulk densification of our suspensions during microchannel flow. We calculate the volume fraction at different positions along the channel by first counting the number of particles in each movie and then correcting for undersampling using eqn (1),[35] and report the bulk volume fraction ϕ normalized by that at the channel entrance, ϕ_{ent}. The colloidal suspension with a weak interparticle attraction ($c_p = 5$ mg mL^{-1}) densifies as it flows through the microchannel, as shown in Fig. 4. As the suspension travels from $x/L = 50$ to 200 channel diameters downstream, the normalized volume fraction ϕ/ϕ_{ent} increases with x/L during flow at a volumetric rate of either 8 μL h^{-1} (as indicated by the open circles) or 10 μL h^{-1} (open triangles). This behavior is in contrast to that observed for dense suspensions near the colloidal glass transition ($\phi \sim 0.5$), which dilate during constricted flow and hence become more dilute due to self-filtration.[37,38,55] Increasing the strength of attraction suppresses the consolidation: for a suspension with $c_p = 25$ mg mL^{-1} (closed circles), the volume fraction increases slightly after entering the channel ($x/L = 50$–80) and then remains nearly constant as the distance downstream is further increased. These differences in densification during microchannel flow must result from the coupling between the local flow profiles and the microstructure of the suspensions, which in turn reflects differences in the strength of the interparticle attraction. To capture these differences, we measure the velocity and local density profiles for each suspension.
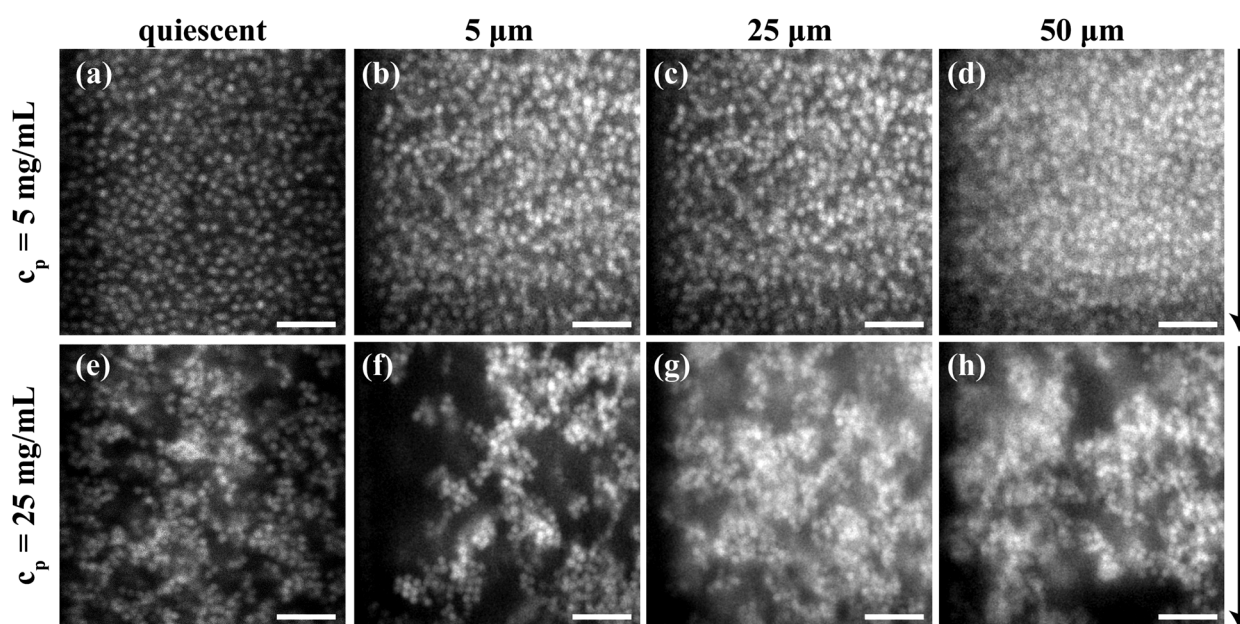

Fig. 3 Confocal micrographs of colloidal suspensions with polymer concentration c_p of (a–d) 5 mg mL^{-1} and (e–h) 25 mg mL^{-1}. Images (a) and (e) show the quiescent sample; images (b–d) and (f–h) were acquired during flow at a height (z) of (b and f) 5 μm, (c and g) 25 μm, and (d and h) 50 μm above the bottom surface of the microchannel. The edge of the channel is at the left-hand side of each image in (b–d) and (f–h), and flow is in the downward vertical direction. The scale bar is 10 μm.

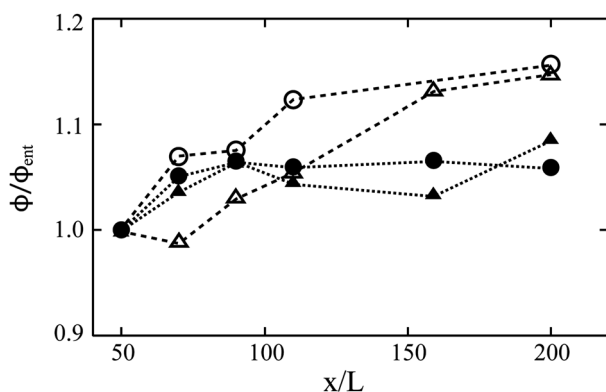**Fig. 4** Normalized bulk volume fraction ϕ/ϕ_{ent} as a function of the normalized distance downstream in the microchannel, x/L, for suspensions with $\phi \approx 0.15$ and $c_p = 5$ mg mL^{-1} (open symbols) or 25 mg mL^{-1} (closed symbols) flowing at a volumetric rate of 8 (triangles) or 10 (circles) µL h^{-1} in a microcapillary with inner diameter 100 µm.

Weak attraction: shear-induced migration and consolidation

We use image correlation algorithms to obtain the velocity of a suspension of weakly attractive particles ($c_p = 5$ mg mL^{-1}) as a function of the lateral distance (y/L) across the microchannel during flow, shown in a representative movie (Movie S1) in ESI.† We normalize the measured advection velocity profiles by the maximum velocity at the midplane of the channel and compare to the velocity profiles expected for a Newtonian fluid flowing in a square microchannel,[56]

$$\frac{U(y,z)}{U_{max}} = \sum_{k=1,3,5...} (-1)^{(k-1)/2} \left[1 - \frac{\cosh(k\pi z/L)}{\cosh(k\pi z/2L)}\right] \frac{\cos(k\pi y/2L)}{k^3}$$

(2)

in which z is the distance from the midplane of the microchannel, L is the width of the channel, h is the microchannel height, and y is the lateral position across the microchannel measured from the center. We find that the velocity profiles of the weakly attractive particles are consistent with Newtonian flow in a microchannel, as shown in Fig. 5; the dashed lines in the figures indicate fits of the normalized velocity profile to eqn (2). Within the errors of the measurement, we observe minimal evolution in the velocity profiles at different downstream positions, as shown for positions $x/L = 50$ and 200 and a volumetric flow rate of 8 µL h^{-1}. In particular, the maximum value of the velocity in the channel, $v_{max} \approx 200$ µm s^{-1}, does not change within experimental error between positions $x/L = 50$ and $x/L = 200$. We obtain similar results for a slightly larger volumetric flow rate of 10 µL h^{-1}.

We further confirm that the flow behavior of this suspension is consistent with Newtonian flow at these flow rates by estimating the shear-zone width of the velocity profiles, defined as the distance from the wall at which the advection velocity is equal to $0.95v_{max}$, where $v_{max}(h)$ is the maximum advection velocity at a height h above the bottom surface of the microchannel.[42] From the velocity profiles, we estimate that the shear-zone width of $\approx 0.80L$ is nearly constant across the flow rates probed close to the entrance of the microchannel ($x/L = 50$), as shown in Fig. 6. This value is close to the theoretical values calculated for Newtonian flow in a square microchannel,[56] which range from
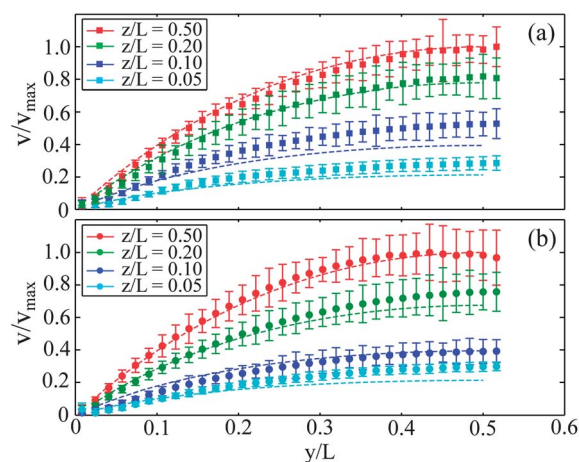

Fig. 5 Normalized velocity profiles as a function of normalized lateral position across the microchannel y/L for the suspension with a weak interparticle attraction (volume fraction $\phi = 0.155$ and $c_p = 5$ mg mL^{-1}) flowing at a volumetric rate 8 µL h^{-1}. The downstream position x/L was (a) 50 or (b) 200. From top to bottom in each panel, velocity profiles were measured at normalized distances above the bottom surface $z/L = 0.05$, 0.10, 0.20, and 0.50. The dotted lines indicate fits to the Newtonian flow profile (eqn (2)).

$\approx 0.75L$ near the midplane of the microchannel to $\approx 0.8L$ near the walls; we speculate that the slight increase in shear zone width observed in the experiment may result from the small interparticle attraction induced by the polymers, which reduces the interparticle repulsion and allows the particles to more readily move past each other. However, at a downstream distance of $x/L = 200$, the shear-zone width abruptly decreases to ≈ 0.65 near the midplane of the channel (for a flow rate of 8 µL h^{-1}) or ≈ 0.72 (for a flow rate of 10 µL h^{-1}). In earlier experimental and modeling studies of the microchannel flow of hard-sphere suspensions, particles migrated in the shear gradient towards the center of the microchannel; the resultant increase in local density there reduced the local shear rate and led to a slight blunting of the flow profiles.[35] We therefore suggest that the decrease in shear zone width observed downstream in our experiments similarly
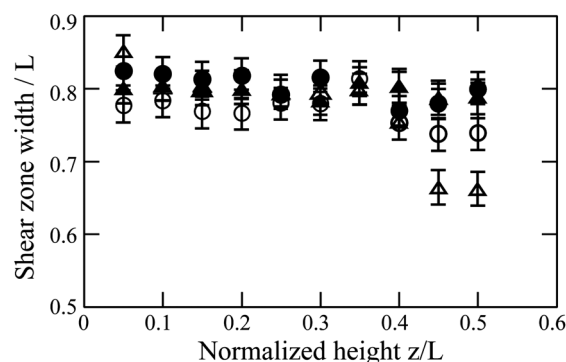

Fig. 6 Shear zone width normalized by L as a function of normalized vertical position across the microchannel z/L for suspension with volume fraction $\phi = 0.15$ and $c_p = 5$ mg mL^{-1}, acquired at flow rates of 8 µL h^{-1} (triangles) and 10 µL h^{-1} (circles). Filled and open symbols respectively indicate measurements taken at downstream position $x/L = 50$ and 200, respectively.

indicates an increase in the local concentration of particles due to shear-induced migration.

The Péclet number $\text{Pe} = (a^2/D)/(1/\dot\gamma)$ is the ratio of the time-scale for a particle to diffuse its diameter a^2/D to the convection timescale $1/\dot\gamma$ and thus measures the relative importance of thermal and shear-driven motion. Particles in the weakly attractive suspension freely diffuse in a quiescent sample, as measured by the single-particle mean-square displacement.[57] We therefore estimate the free diffusion coefficient for the particles as $D = k_B T/6\pi\eta a$ using the viscosity η of a polymer solution at concentration $c_p = 5$ mg mL^{-1}, $\eta \approx 0.006$ Pa s. For a volumetric flow rate of 8 μL h^{-1}, the shear rate across the microchannel is $\dot\gamma \approx V_{max}/(L/2) \approx 4$ s^{-1} (using a maximum velocity $V_{max} \approx 200$ μm s^{-1} from Fig. 5). This value of the shear rate is firmly within the high-shear plateau region of the flow curve shown in Fig. 2. Finally, we estimate $\text{Pe} = 6\pi\eta a^3\dot\gamma/k_B T \approx 50$. The previous work of Semwogerere et al.[35] on the shear-induced migration of hard-sphere colloids predicts that the entrance length at $\text{Pe} \approx 50$ is quite short, of order $\mathscr{O}(100)L$; we assume that the interparticle attraction is sufficiently small so that the earlier results on nearly hard-spheres can be applied to our system.

We directly determine the extent of shear-induced migration by measuring the distribution of particles across the channel (as a function of the normalized lateral distance y/L) at different heights (z/L) during flow. The number of particles increases towards the center of the channel, shown for density profiles acquired at two different downstream distances ($x/L = 50$ and 200) for a flow rate of 10 μL h^{-1} in Fig. 7, and is consistent with shear-induced migration. Close to the entrance of the channel ($x/L = 50$), the increase in particle number from the lateral edge to the center of the channel is most pronounced near the midplane of the microchannel, where particles are especially depleted near the walls of the channel: at $z/L = 0.50$, the slope of the density profile is 0.34 particles per μm, whereas at the bottom of the channel ($z/L = 0.05$) the slope is 0.04 particles per μm. Comparison of the density profiles at x/L indicates that that the number of particles increases downstream at every position across the microchannel (y/L), and the slopes of the density profiles are comparable at both positions: for example, the slopes at $x/L = 200$ and $z/L = 0.05$ and 0.50 are 0.06 and 0.22 particles per μm, respectively. Similar results are obtained at flow rates of 8 and 15 μL h^{-1}. Very local measurements of density, obtained by averaging the fluorescence intensity of the images at constant lateral distance across the microchannel (y/L) over time and along the direction of flow, reveal well-defined and periodic local maxima near walls consistent with the formation of layers of particles (as shown for representative data in Fig. S3 in ESI†). By counting the number of distinct maxima in the average intensity for the ten different heights at which we acquire movies, we find that 3–6 layers form near the lateral wall at a flow rate of 8 μL h^{-1} and 2–9 layers form at a flow rate of 15 μL h^{-1}; within measurement errors the number of layers is constant at different downstream positions along the channel. The local density measurements confirm that suspensions with a weak interparticle attraction undergo shear-induced migration, as suggested by the velocity profiles, and densification, as suggested by the bulk density measurements.

Strong attraction: clustering resists shear-induced changes in microstructure

The velocity profiles of a suspension of particles that interact via a strong attraction ($c_p = 25$ mg mL^{-1}) exhibit distinct features from those of the weakly attractive ($c_p = 5$ mg mL^{-1}) suspension. First, the velocity profiles obtained at a flow rate of 8 μL h^{-1} exhibit significant deviations from the Newtonian flow profiles calculated from eqn (2), as shown in Fig. 8. Second, the velocity profiles for the strongly attractive suspension evolve as they flow through the microchannel: for example, the maximum velocity close to the entrance of the microcapillary (at $x/L = 50$, $v_{max} \approx 240$ μm s^{-1}) is significantly larger than that measured further downstream (at $x/L = 200$, $v_{max} \approx 200$ μm s^{-1}). These changes may reflect an increase in entrance effects due to the high Péclet
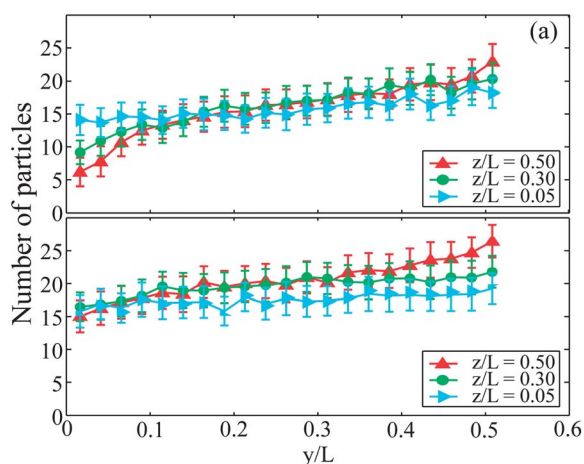

Fig. 7 Number of particles as a function of normalized lateral position across the microchannel y/L for suspension with volume fraction $\phi = 0.15$ and $c_p = 5$ mg mL^{-1} flowing at 10 μL h^{-1}, acquired at downstream position $x/L = $ (a) 50 and (b) 200, for three normalized heights $z/L = 0.05$ ($\triangle$), 0.30 ($\bigcirc$), 0.50 ($\triangleright$). The lines shown are guides to the eye.
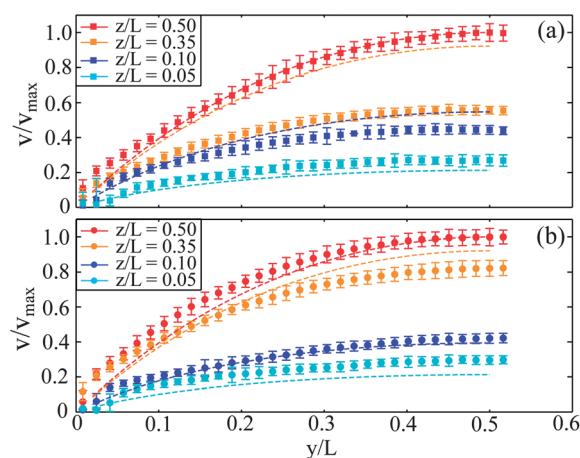

Fig. 8 Normalized velocity profiles as a function of normalized lateral position across the microchannel y/L for suspension with volume fraction $\phi = 0.15$ and $c_p = 25$ mg mL^{-1}, acquired at downstream position $x/L = $ (a) 50 and (b) 200. From top to bottom in each panel, velocity profiles were measured at heights $z/L = 0.05, 0.10, 0.35, 0.50$. The flow rate was 8 μL h^{-1}. The dotted lines indicate fits to the Newtonian flow profile (eqn (2)).

number of these flows. In quiescent conditions particles in the strongly attractive suspension are dynamically arrested and typically move less than one diameter in ten minutes (based on quiescent mean-square-displacement measurements). We thus estimate the maximum diffusion coefficient $D = (2a)^2/(600\text{ s}) \approx 4 \times 10^{-3}\ \mu\text{m}^2\ \text{s}^{-1}$ and thereby obtain a lower bound on the Péclet number Pe ≈ 720. Comparison to the entrance length data of Semwogerere et al.[35] indicate that the entrance lengths for this sample are of order $\sim \mathcal{O}(1000L)$ and are independent of Péclet number for Pe $> 10^3$; these lengths are longer than the length of the microcapillary used in these experiments. Finally, the magnitudes of the velocities near the wall exhibit increased variance when the interparticle attraction is stronger, and are nonzero at the lateral edge ($y/L = 0$), indicating slip consistent with that observed in the bulk rheology measurements (Fig. 2). The differences in the shape of these profiles with increased attraction are reflected in the evolution of the shear zone width across the microchannel, as shown in Fig. 9. The shear-zone width decreases monotonically towards the midplane of the microchannel and does not evolve as the suspension flows downstream through the channel. The value of the shear zone width near the center of the channel for the strongly attractive suspension at all flow rates and downstream positions ($\approx 0.68\ L$) is comparable to that found for the jammed suspension in the weakly attractive system. Increasing the strength of attraction increases the strength of the bonds between particles, which resist the shear forces applied by the flow. In the strongly attractive suspension the continuous decrease in the shear zone width with height thus reflects reduced yielding as the shear stress applied by flow is decreased; by contrast in the weakly attractive suspension the discontinuous decrease reflects the onset of jammed behavior once a threshold volume fraction is reached.

To uncover the microstructural origins of the differences in the flow profiles due to increasing strength of attraction, we first examine the number density profiles across the microchannel. The steepest gradient in particle density occurs near the bottom of the microchannel, at a normalized height of $z/L = 0.05$ as shown in Fig. 10; this variation is in contrast to that observed in
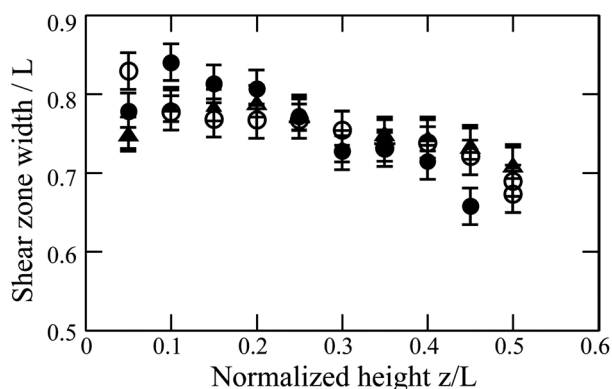
the weakly attractive suspension, in which the steepest gradient was observed near the midplane ($z/L = 0.50$), and is not understood. Away from the bottom surface of the microchannel, the increase in number density across the microchannel is less than that in the weakly attractive suspension, as quantified by the slope of the density profile: for example, at heights of $z/L = 0.30$ and 0.50, the slopes of the number density profile at a position $x/L = 50$ are 0.1 and 0.6 particles per μm, respectively (compared to 0.24 and 0.34 particles per μm for the weakly attractive suspension). We obtain similar results for flow rates of 8 and 15 μL h^{-1}. These profiles indicate that the stronger attraction between the particles suppresses the shear-induced migration seen in more weakly attractive suspensions that leads to increased concentration near the center of the microchannel. Moreover, the number density does not increase after a short entrance distance due to the increase in compressive yield stress P_y, which scales with the shear yield stress as $P_y \approx 55\sigma_y$ for colloidal gels.[58] Using this scaling, we estimate that the compressive yield stress for the strongly attractive suspension is $P_y \approx 2$ Pa. The viscous stress at a given flow rate can be estimated using the constitutive model for a Herschel–Bulkley fluid as $\sigma_v = k(V_{max}/L)^n$, where V_{max} is the maximum advection velocity in the channel and k and n are the parameters determined from the viscometry stress data in Fig. 2. Using the maximum velocity $V_{max} \approx 200\ \mu\text{m s}^{-1}$ at the flow rate of 8 μL h^{-1}, we estimate $\sigma_v \approx 0.14$ Pa and therefore the stress imparted by the flow is insufficient to cause compressive yielding. By contrast, for the weakly attractive suspension the magnitude of the viscous stress ($\sigma_v \approx 0.02$ Pa) is comparable to the estimated compressive yield stress ($P_y \approx 0.03$), suggesting that the small interparticle attraction in the weakly attractive suspension cannot resist consolidation via compression.

The mechanisms of yielding during flow also evolve as the strength of attraction is increased: yielding occurs at the low shear rates studied here by the breaking of bonds between
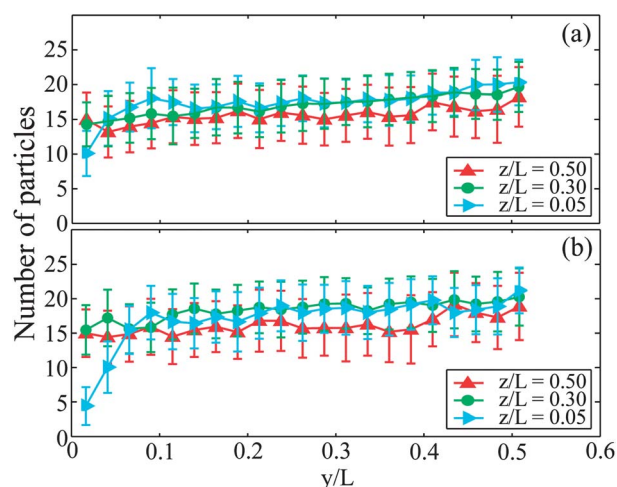

Fig. 9 Shear zone width normalized by L as a function of normalized vertical position across the microchannel z/L for suspension with volume fraction $\phi = 0.15$ and $c_p = 25$ mg mL^{-1}, acquired at flow rates of 8 μL h^{-1} (triangles) and 10 μL h^{-1} (circles). Filled and open symbols respectively indicate measurements taken at downstream position $x/L = 50$ and 200, respectively.

Fig. 10 Number of particles as a function of normalized lateral position across the microchannel y/L for suspension with volume fraction $\phi = 0.15$ and $c_p = 25$ mg mL^{-1} flowing at 10 μL h^{-1}, acquired at downstream position $x/L =$ (a) 50 and (b) 200, for three normalized heights above the bottom of the microchannel $z/L = 0.05$ ($\triangle$), 0.30 ($\bigcirc$), 0.50 ($\triangleright$). The lines shown are guides to the eye.

clusters of particles as shown in Movie S2 in ESI.† The number of bonds between two clusters is smaller than the average number of nearest-neighbor bonds for a particle inside a cluster;[14] therefore, yielding occurs at these relatively weak points in the gel network, as previously seen for colloidal gels flowing under an applied electric field.[59] A typical cluster contains many particles and hence its diameter is much larger than that of a single particle. The shear gradient near the wall therefore induces a tumbling rotation of clusters that opposes the direction of flow and leads to greater variance in velocity near the walls. We estimate the size of the region of tumbling clusters in each two-dimensional movie, corresponding to a particular height in the microchannel, from the fluorescence intensity across the micro-channel (along the y direction) averaged over all frames in the movie: near the edge of the wall, the average intensity is significantly lower as clusters are excluded by their size from the wall, whereas near the center the distribution of clusters is nearly uniform and the fluorescence intensity is approximately constant. The intensity does not contain the distinct maxima that indicate layering of particles, as seen for the weakly attractive suspension, but instead exhibits a second local minimum whose position indicates the edge of the region of tumbling clusters and hence the maximum size of such clusters. We numerically differentiate the intensity profile to determine the position of the second local minimum and summarize the results in Fig. 11. The width of the region of tumbling clusters decreases with increasing flow rate, consistent with the increase in disruption of intercluster and interparticle bonds at higher shear rates as measured using bulk rheology. Notably, the width of this region also decreases downstream in the microchannel (Fig. 11(b)), indicating that the viscous stresses continue to break and reshape clusters as the suspension flows the microchannel. Although the increase in strength of attraction suppresses shear-induced migration and densification, confined microchannel flow nonetheless continues to affect the distribution of cluster sizes along the channel due to the complex interactions and yielding of clusters near the walls.
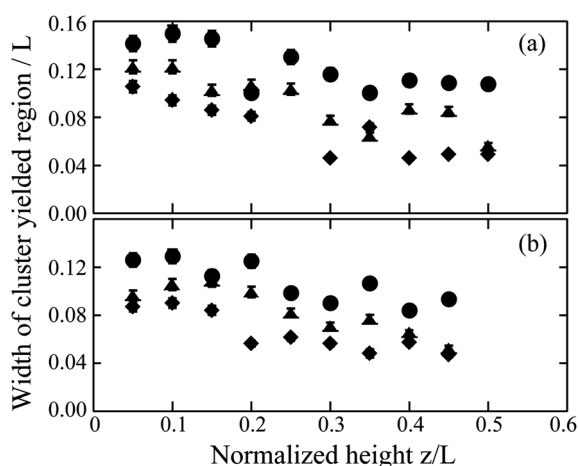
Conclusions

We investigated the flow of weakly and strongly model colloid–polymer mixtures in confined geometries using microfluidics. Increasing the strength of attraction *via* the concentration of the polymer depletant does not modify the magnitude of the flow velocities, but instead changes the shape of the flow profiles. Notably, the velocity profiles near the edges of the microchannel are modified by an increase in the interparticle attraction that reflects changes in the local arrangement of particles. In a weakly attractive suspension, the particles are unable to resist consolidation by compression during the flow, and the shear gradient drives shear-induced migration of particles that leads to densification near the center of the channel. The combination of these effects drives an increase in the density downstream in the microchannel. By contrast, the increased strength of bonds between particles leads to the formation of clusters that readily yield at weak points with few nearest-neighbor bonds. The clusters resist shear-induced migration over short lengths and resist consolidation by the increase in compressive yield stress; nonetheless, complex interactions between clusters and the walls lead to changes in the structure of the clusters as the suspension flows through the channel. Our experiments provide new metrics by which to quantify the influence of walls on the microstructure of attractive suspensions flowing in microchannels. The relationships between rheology and microstructure identified here may provide new insight into the physics of other confined flow phenomena in two and three dimensions, and thereby guide the design of colloidal suspensions for technological applications that require colloidal suspensions to be extruded or flowed through fine geometries.

Acknowledgements

Fig. 11 Width of the region of tumbling clusters normalized by L as a function of the normalized height in the microchannel z/L for a strongly attractive suspension with $c_p = 25$ mg mL^{-1} at a volumetric flow of 8 μL h^{-1} (circles), 10 μL h^{-1} (triangles), or 15 μL h^{-1} (diamonds), acquired at a downstream distance of (a) $x/L = 50$ or (b) $x/L = 200$. The experimental error on the measurements is comparable to the size of the symbols.

References

1 D. P. Kalman and N. J. Wagner, *Rheol. Acta*, 2009, **48**, 897–908.
2 C. Gao, S. D. Kulkarni, J. F. Morris and J. F. Gilchrist, *Phys. Rev. E: Stat., Nonlinear, Soft Matter Phys.*, 2010, **81**, 041403.
3 X. Cheng, J. H. McCoy, J. N. Israelachvili and I. Cohen, *Science*, 2011, **333**, 1276–1279.
4 V. Gopalakrishnan and C. F. Zukoski, *J. Rheol.*, 2004, **48**, 1321–1344.
5 S. A. Shah, Y. L. Chen, K. S. Schweizer and C. F. Zukoski, *J. Chem. Phys.*, 2003, **119**, 8747–8760.
6 V. Prasad, V. Trappe, A. D. Dinsmore, P. N. Sègre, L. Cipelletti and D. A. Weitz, *Faraday Discuss.*, 2003, **123**, 1–12.
7 V. L. Kobelev and K. S. Schweizer, *J. Chem. Phys.*, 2005, **123**, 164902.
8 N. Koumakis and G. Petekidis, *Soft Matter*, 2011, **7**, 2456–2470.
9 R. Buscall, I. J. McGowen and A. J. Morton-Jones, *J. Rheol.*, 1993, **37**, 621–641.
10 S. Ramakrishnan, Y. L. Chen, K. S. Schweizer and C. F. Zukoski, *Phys. Rev. E: Stat., Nonlinear, Soft Matter Phys.*, 2004, **70**, 040401.
11 P. J. Lu, J. C. Conrad, H. M. Wyss, A. B. Schofield and D. A. Weitz, *Phys. Rev. Lett.*, 2006, **96**, 028306.
12 M. Laurati, S. U. Egelhaaf and G. Petekidis, *J. Rheol.*, 2011, **55**, 673–706.
13 M. Laurati, G. Petekidis, N. Koumakis, F. Cardinaux, A. B. Schofield, J. M. Brader, M. Fuchs and S. U. Egelhaaf, *J. Chem. Phys.*, 2009, **130**, 134907.

14 J. C. Conrad, H. M. Wyss, V. Trappe, S. Manley, K. Miyazaki, L. J. Kaufman, A. B. Schofield, D. R. Reichman and D. A. Weitz, *J. Rheol.*, 2010, **54**, 421–438.

15 J. J. Stickel and R. L. Powell, *Annu. Rev. Fluid Mech.*, 2005, **37**, 129–149.

16 J. Mewis and N. J. Wagner, *J. Non-Newtonian Fluid Mech.*, 2009, **157**, 147–150.

17 J. F. Morris, *Rheol. Acta*, 2009, **48**, 909–923.

18 J. M. Brader, *J. Phys.: Condens. Matter*, 2010, **22**, 363101.

19 S. B. Fuller, E. J. Wilhelm and J. M. Jacobson, *J. Microelectromech. Syst.*, 2002, **11**, 54–60.

20 T. H. J. van Osch, J. Perelaer, A. W. M. de Laat and U. S. Schubert, *Adv. Mater.*, 2008, **20**, 343–345.

21 B.-Y. Ahn, E. Duoss, M. J. Motala, X. Guo, S. Park, Y. Xiong, J. Yoon, R. G. Nuzzo, J. A. Rogers and J. A. Lewis, *Science*, 2009, **323**, 1590–1593.

22 M. Duduta, B. Ho, V. C. Wood, P. Limthongkul, V. E. Brunini, W. C. Carter and Y.-M. Chiang, *Adv. Energy Mater.*, 2011, **1**, 511–516.

23 J. Philip, P. D. Shima and B. Raj, *Nanotechnology*, 2008, **19**, 305706.

24 P. Gharagozloo and K. Goodson, *J. Appl. Phys.*, 2010, **108**, 074309.

25 H. J. Walls, S. B. Caines, A. M. Sanchez and S. A. Khan, *J. Rheol.*, 2003, **47**, 847–868.

26 D. M. Kalyon, *J. Rheol.*, 2005, **49**, 621–640.

27 H. M. Wyss, D. L. Blair, J. F. Morris, H. A. Stone and D. A. Weitz, *Phys. Rev. E: Stat., Nonlinear, Soft Matter Phys.*, 2006, **74**, 061402.

28 L. Xu, S. Davies, A. B. Schofield and D. A. Weitz, *Phys. Rev. Lett.*, 2008, **101**, 094502.

29 K. Xu, A. Bergès, P. J. Lu, A. R. Studart, A. B. Schofield, H. Oki, S. Davies and D. A. Weitz, *Phys. Rev. Lett.*, 2010, **104**, 128303.

30 T. M. Squires and S. R. Quake, *Rev. Mod. Phys.*, 2005, **77**, 977–1026.

31 M. Frank, D. Anderson, E. R. Weeks and J. F. Morris, *J. Fluid Mech.*, 2003, **493**, 363–378.

32 Y. Xia and G. M. Whitesides, *Annu. Rev. Mater. Sci.*, 1998, **28**, 153–184.

33 K. J. Humphry, P. M. Kulkarni, D. A. Weitz, J. F. Morris and H. A. Stone, *Phys. Fluids*, 2010, **22**, 081703.

34 V. Prasad, D. Semwogerere and E. R. Weeks, *J. Phys.: Condens. Matter*, 2007, **19**, 113102.

35 D. Semwogerere, J. F. Morris and E. R. Weeks, *J. Fluid Mech.*, 2007, **581**, 437–451.

36 D. Semwogerere and E. R. Weeks, *Phys. Fluids*, 2008, **20**, 043306.

37 M. D. Haw, *Phys. Rev. Lett.*, 2004, **92**, 185506.

38 A. I. Campbell and M. D. Haw, *Soft Matter*, 2010, **6**, 4688–4693.

39 L. Isa, R. Besseling, A. Morozov and W. C. K. Poon, *Phys. Rev. Lett.*, 2009, **102**, 058302.

40 D. Genovese and J. Sprakel, *Soft Matter*, 2011, **7**, 3889–3896.

41 K. N. Nordstrom, E. Verneuil, P. E. Arratia, A. Basu, Z. Zhang, A. G. Yodh, J. P. Gollub and D. J. Durian, *Phys. Rev. Lett.*, 2010, **105**, 175701.

42 M. T. Roberts, A. Mohraz, K. T. Christensen and J. A. Lewis, *Langmuir*, 2007, **23**, 8726–8731.

43 J. C. Conrad and J. A. Lewis, *Langmuir*, 2008, **24**, 7628–7634.

44 J. C. Conrad and J. A. Lewis, *Langmuir*, 2010, **26**, 6102–6107.

45 P. N. Pusey and W. van Megen, *Nature*, 1986, **320**, 340–342.

46 L. Antl, J. W. Goodwin, R. D. Hill, R. H. Ottewill, S. M. Owens, S. Papworth and J. A. Waters, *Colloids Surf.*, 1986, **17**, 67–78.

47 A. Yethiraj and A. van Blaaderen, *Nature*, 2003, **421**, 513–517.

48 G. C. Berry, *J. Chem. Phys.*, 1966, **44**, 4550–4564.

49 S. M. Ilett, A. Orrock, W. C. K. Poon and P. N. Pusey, *Phys. Rev. E: Stat. Phys., Plasmas, Fluids, Relat. Interdiscip. Top.*, 1995, **51**, 1344–1352.

50 J. C. Crocker and D. G. Grier, *J. Colloid Interface Sci.*, 1996, **179**, 298–310.

51 http://physics.georgetown.edu/matlab/.

52 R. Besseling, L. Isa, E. R. Weeks and W. C. K. Poon, *Adv. Colloid Interface Sci.*, 2009, **146**, 1–17.

53 W. H. Bulkley and A. R. Herschel, *Kolloidn. Z.*, 1926, **39**, 291–300.

54 S. Manley, J. M. Skotheim, L. Mahadevan and D. A. Weitz, *Phys. Rev. Lett.*, 2005, **94**, 218302.

55 S. D. Kulkarni, B. Metzger and J. F. Morris, *Phys. Rev. E: Stat., Nonlinear, Soft Matter Phys.*, 2010, **82**, 010402.

56 F. M. White, *Viscous Fluid Flow*, McGraw-Hill, 3rd edn, 2006.

57 M. Spannuth and J. C. Conrad, *Phys. Rev. Lett.*, 2012, **109**, 028301.

58 G. M. Channell and C. F. Zukoski, *AIChE J.*, 1997, **43**, 1700–1708.

59 M. Kogan and M. J. Solomon, *Langmuir*, 2010, **26**, 1207–1213.

60 B. Rajaram and A. Mohraz, *Soft Matter*, 2010, **6**, 2246–2259.

61 B. Rajaram and A. Mohraz, *Phys. Rev. E: Stat., Nonlinear, Soft Matter Phys.*, 2011, **84**, 011405.